A review on phosphide based material for electro-catalytic hydrogen evolution

Peng Xiao,[a] *Wei Chen,*[b] *Xin Wang**[a]

[a] School of Chemical and Biomedical Engineering, Nanyang Technological University, 62 Nanyang Drive, 637459 Singapore

[b] Departments of Chemistry & Physics, National University of Singapore, 3 Science Drive 3, Singapore 117543

* Corresponding author. E-mail: WangXin@ntu.edu.sg; Fax: +65 67947553

Abstract

Hydrogen evolution by means of electro-catalytic water-splitting is pivotal for efficient and economical production of hydrogen, which relies on the development of inexpensive, highly active catalysts. Aside from sulfides, the search for non-noble metal catalysts has been mainly directed at phosphides due to the superb activity of phosphides towards hydrogen evolution reaction (HER) and low-cost considering the abundance of the non-noble constituents of phosphides. In this review article, recent works of phosphides are summarized based on their synthetic methodology. A comparative study of the catalytic activity of different phosphides towards HER is then conducted. The catalytic activity herein is evaluated by overpotentials at fixed current density (*e.g.*, 10 mA cm^{-2}), Tafel slope, turnover frequency and Gibbs free energy of hydrogen adsorption. On the ground of the established methods, we provide our perspective on pros and cons of various methods for phosphides synthesis, and discuss the origins of their high activities and the role of phosphorus on the improved activity towards HER.

Keywords: hydrogen evolution reaction, non-noble metal catalyst, phosphide, water splitting, electrocatalysis

1. Introduction

There is a pressing need to explore new forms of energy and energy carriers to reduce fossil fuel dependency and carbon footprint in the long term. Molecular hydrogen shows great promise as an energy carrier as it is both carbon-free and environmentally friendly. Hydrogen evolution reaction (HER) *via* electro-catalysis from renewable energy is a potentially viable way to produce hydrogen economically and efficiently when an inexpensive and active catalyst is applied. Currently, the most effective catalyst for the HER under acidic condition is well known to be Pt. Unfortunately, the high cost and limited availability of Pt prohibit its large-scale application in water electro-splitting devices. Thus, the development of novel cost-effective and earth abundant catalysts with high activity as Pt substitutes is desired.

Two dimensional layer-structured MoS_2 has emerged as one candidate to replace Pt as it possesses promising activity for HER when nano-scaled MoS_2 is applied [1], albeit bulk MoS_2 is suggested to be inactive towards HER [2]. Thus most studies have focused on designing thin layered/nanostructured MoS_2 nanomaterials with most exposed edges for HER. To this end, amorphous MoS_2 [3], MoS_x nanosheets [4] were found to outperform bulk MoS_2 significantly; layer-dependent attributes [5], the correlation with intrinsic low conductivity out-of-plane, and phase-determined performance have also been studied [6]. These findings have stimulated the work of sulfide of earth-abundant metals, *e.g.* WS_2 [7], and its analogue – selenides [8], resulting in a big family of chalcogenides of first-row transition metals [9]. Reviews [6b, 7c, 10] have been conducted from different perspectives, and can be referred to accordingly. Unfortunately, the best performing MoS_2 catalyst still lacks the competitiveness of Pt. Furthermore, improvements in performance relies heavily on the basis that molybdenum/tungsten chalcogenides (sulfide, selenide) are nano-

structured with abundant S-edges and are thin layered (preferable single layer). These requirements may severely constrain their application in large-scale production. Thus, it is imperative to continue the search for new inexpensive catalysts that can rival the performance of Pt whilst being suitable for large-scale hydrogen production.

Not until recently, it was discovered that hydrogen evolution undergoes a similar pathway to that of hydrogenation (hydrotreating process), *e.g.*, hydrodesulfurization (HDS) proceeds, where a reversible ad/desorption of hydrogen on catalyst is critical for achieving fast kinetics. This correlation broadens the scope of search for new catalysts. Hence, phosphides, previously employed as catalysts for HDS, were found to be active towards HER, *e.g.*, Ni_2P [11] has been reported to achieve a better performance than the state-of-the-art MoS_2 [11c]. This pivotal work [11c] was followed by a variety of studies applying phosphide as catalysts for HER. This class of electro-catalyst with superb electro-catalytic activities has thus opened up a new avenue in the search of non-noble metal catalysts for HER.

In this article, we focus our discussion on the recent developments of synthesis methodology of phosphides for HER. Based on different synthetic routes of phosphides, we then make a comparative survey of their activities, which are evaluated in terms of experimental metrics of over-potential (η) at a certain current density (j), Tafel slope coupled with exchange current density (j_o) extrapolated from the plot of η *vs.* Log_{10} (j), and turnover frequency (TOF). In conjunction with experimental results, theoretical calculations concerning the active sites and the origins of the activity will also be discussed on the basis of the Gibbs free energy (ΔG) of the ad/desorption of hydrogen (H*) on the catalyst.

2. Mechanism and the origin of activities

Hydrogen evolution reaction (HER) in acidic medium involves the following steps.

Volmer: $H^+ + e^- + Cat \leftrightharpoons Cat\text{-}H$ (1)

Heyrovsky: $H^+ + e^- + Cat\text{-}H \leftrightharpoons H_2 + Cat$ (2)

Tafel: $Cat\text{-}H + Cat\text{-}H \leftrightharpoons H_2 + 2Cat$ (3)

, where Cat is a short term for catalyst, and Cat-H represents adsorbed hydrogen atom on the catalyst. Mechanistic study of HER suggests that a molecular H_2 can be formed *via* two pathways – Volmer-Heyrovsky or Volmer-Tafel. The generally recognized three sub-reactions have classically described how aqueous protons evolve to H_2 by engaging a catalyst and the protons. More importantly, this mechanism successfully bridges experimental data and theoretical calculations. In experiment, linear scanning voltammetry (LSV) that shows the response of current density to the applied potential (typically in a three-electrode setup), could be interpreted as overpotential η *vs. Logarithm* (j), and the Tafel slope can be derived from the linear part. The Tafel slope of 30, 40 and 120 mV dec^{-1} is designated to Tafel, Herovsky, and Volmer reaction respectively, and functions as a metric to assess the sample catalyst, unveiling the rate-determining steps (RDS) in HER. In theory, transformation of Cat-H to/from Cat shown in reaction (1), (2) and (3), can be described from the thermodynamic viewpoint, that is, the repeatedly electrochemical replenishing of catalyst with H means a reversible ad/desorption of hydrogen on the active sites, and the Gibbs free energy ($\Delta G_{cat\text{-}H}$) of ad/desorption can be obtained by density functional theory (DFT) on selectively constructed facets of catalysts [12].

$$\Delta G_{cat\text{-}H} = \Delta E_{cat\text{-}H} + \Delta E_{ZPE} - T\Delta S_H \quad (5)$$

, where $\Delta E_{cat\text{-}H}$ is the differential hydrogen chemisorption energy, ΔE_{ZPE} is the difference of the zero-point energy between the adsorbed H and isolated one, ΔS_H is

the entropy change in ad/desorption, and T is the temperature. In accordance with Sabatier's principle [13] that a good catalyst should bind hydrogen neither too strongly nor too weakly, $\Delta G_{\text{cat-H}}$ would ideally be zero for selected catalysts. Conforming to this principle, Nørskov et al. [12b] investigated the origins of activities of hydrogen evolution reaction on a collection of metals, and introduced a 'volcano plot' that reveals the hierarchical kinetics among metals. For instance, metal Mo locates in bottom-left of the 'volcano plot' is a poor catalyst for HER because of the strong bonding strength to hydrogen that makes the reversible desorption of hydrogen hard to be realized; nearly thermo-neutral Pt-group metals were the optimum. Jaramillo et al. [1] found that the exchange current density of MoS_2 which is obtained from annealing Mo in H_2S is improved by two orders of magnitude compared to the pure metal Mo and the Gibbs free energy of adsorption of hydrogen is close to zero, as shown in Figure 1. This phenomenon is analogous to HDS reaction that relies on adsorption of organosulfur and H_2 molecule on the catalyst, desorption of hydrocarbon fragments and as-formed H_2S [11a, 14]; and the removal of C-S fragments and S adatoms are very difficult on metals, *e.g.* Ni, Mo [15]. Early investigation of phosphides uncovered a higher activity towards HDS compared with their metal counterpart [16]. Later, a study of Ni_2P by Liu et al. [11a] proposed a 'ligand effect' of P to Ni that facilitates the removal of S-adatoms and delivery of hydrogen by providing a moderate bonding to intermediate products. It was found that this moderate bonding strength to hydrogen by P ligand (so-called "ensemble effect") in phosphides existing in HER, is pivotal for delivering molecular H_2 and reducing H-poisoning effect. A case study of MoP based on theoretical calculation [17] also gives emphasis on P site by showing that $\Delta G_{\text{cat-H}}$ on (001)-P terminated plane could approach zero at the H coverage of 50 % to 75%. Other studies [18] assign P as a proton acceptor based on the

electron-distribution, *i.e*, negative-charged P would potentially bond proton. The calculation of density of state (DOS) also confirms a close-to-Femi-level d-band electron density on (001) of Ni_2P where P sites are readily exposed [19]. It is noteworthy that in the case of Ni_2P, the first H is on the threefold Ni site or P hollow site in terms of the adsorption energy, -0.357 eV (Figure 2), followed by the Ni-P bridge site for the second H (-0.14 eV) [20]. In contrast, top Ni in Ni_2P [20] and Mo-Mo bridge site in MoP [17] are found not favored, that is, H tends to move to hollow P site. To complete the hydrogen evolution reaction, adsorbed hydrogen atoms are to diffuse for the combination to form molecular hydrogen, which involves various pathways, but essentially is to overcome the transitional energy (G^{TS}). Thus, G^{TS} is kinetically correlated with the exchange current density that is used to experimentally select good catalyst. On the contrary to previous conclusion that the (001) facet is speculated to be the most active facet, Hu et al. renders ($\bar{1}\,\bar{1}\,20$) facet and the ($11\bar{2}\,0$) as more active facets [20] based on the energy barrier - G^{TS}. Note that the geometry of surface with adsorbed H atoms plays a critical role in determining G^{TS}, which makes the conclusion not universally applicable.

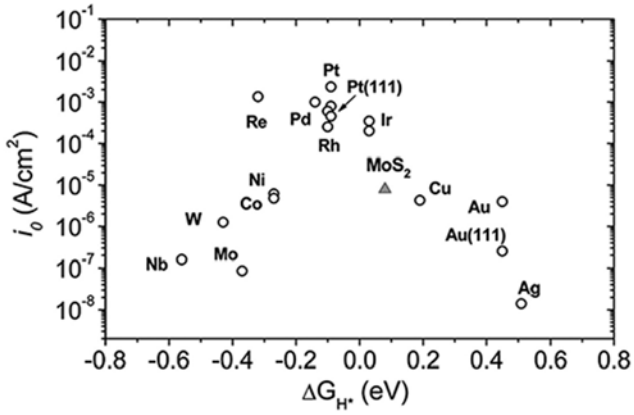

Figure 1 A volcano plot of exchange current density *vs.* Gibbs free energy of adsorption of hydrogen on individual catalyst. Reproduced with permission.[1]. Copyright 2007, American Association for the Advancement Science (AAAS)

Theoretically, it is believed that phosphorus, via 'ensemble effect', has played an important role not only as a proton-acceptor to initiate the HER, but also affecting the metal part by weakening the bond strength to adsorbed hydrogen. Synergistically, the metal moiety is indispensable in H-H bond formation as a hydride acceptor to complete HER. Yet, the exact mechanistic pathways of how HER proceeds vary in different cases, considering the complexity of the process that includes the adsorption of H, its diffusion, recombination and final release from catalyst, as well as different stoichiometric phosphides constructed with different crystal structures. In this regard, a sole indicator based on hydrogen adsorption energy ($\Delta G_{cat\text{-}H}$) may not be convincing enough to pinpoint a good catalyst. Given this, further theoretical calculation would be necessary and insightful in order to understand the significance of metal & phosphorus as well as the synergy between them, and eventually provide guidance for the design of phosphide catalysts with optimal activity.

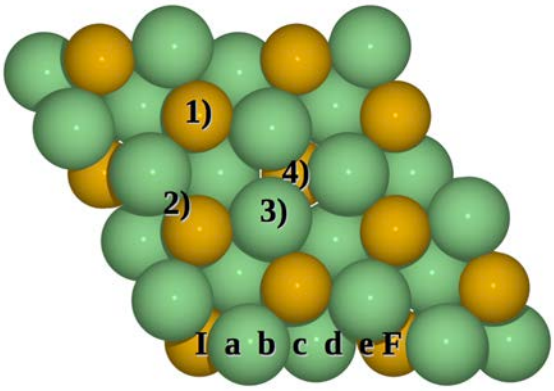

Figure 2 (001) facet of Ni_2P, on which 1) is top P site; 2) is Ni-P bridge site; 3) is Ni top site; 4) is threefold Ni site or hollow P site; a-e are nudged elastic band calculation; I and F denotes the initial and final state on the metal hollow site on the second layer of P atoms. Reproduced with permission.[20] Copyright 2015, Royal Society of Chemistry

3. Synthesis of phosphides and the performance on HER

Generally, the synthesis of phosphide can be categorized by the use of phosphorus source [21]. As far as the application in HER is concerned, phosphorus source is mainly provided from (1) organic phosphine, *e.g.*, trioctyl phosphine, (2) inorganics, *e.g.* phosphate, or (3) in-situ generated PH_3. Different synthetic routes would result in distinct morphology and particle size that bring pronounced impact to the activity of phosphides towards HER.

3.1. Organic phosphine

Prior to the discovery of the activity of phosphides towards HER, a general approach to synthesize phosphide by using trioctylphosphine (TOP) as phosphorus source in organic solvent has been established. Phosphides can be obtained through either thermal decomposition of metal-phosphine complex in organic mixture, *e.g.* MnP [22], or converting as-formed metal nano-particles to phosphide in hot TOP organic solutions [23] at the temperature of 220 to ~385 °C. Besides, controlled compositions, *i.e.*, metal-rich or phosphorus-rich, are achievable by varying the reaction time/temperature or employing inversed cannulation of metal-nanoparticle/hot TOP [24]. It was developed as a general approach for the synthesis of phosphides applicable to a wide range of transition metals – 3d, 4d, 5d including Ni_2P, FeP, palladium phosphide, platinum phosphide. The resultant nanoparticles/nanorods with a particle size ranging from several nm to ~20 nm bear attractive attributes of good uniformity and crystallinity, well-defined nanostructures that are potentially ideal for electro-catalysis. Schaak et al. applied this approach for Ni_2P and measured its activity towards HER in acidic medium for the first time [11c], and found Ni_2P delivers an excellent HER activity, evidenced by low onset potential, low Tafel slope and high exchange current density. As shown in Figure 3a, to reach 20 mA cm^{-2} and 100 mA

cm^{-2}, it only requires an overpotential (η) of 130 mV and 180 mV respectively. This performance compares favorably to MoS_2 [25] and Mo_2C [26]. Later, the same approach is applied to other earth-abundant transition metals and has uncovered a bunch of highly active phosphides – CoP [27], MoP [28], WP [29], FeP [30]. Among these phosphides that are prepared using the same approach, they all exhibit two features (1) nanoparticle shaped (Figure 3a for Ni_2P), size ranging from 13 nm (FeP) to 3 nm (WP), and (2) similar Tafel slopes (46 – 50 mV dec^{-1}), but the activity varies and follows the order of FeP > CoP > MoP > WP ≈ Ni_2P at the same mass loading, ~ 1 mg cm^{-2}. Here, the activity is based on the current density at a fixed potential and exchange current density. For example, FeP and CoP have achieved a high exchange current density of 4.3 $\times 10^{-1}$ mA cm^{-2} and 1.4 $\times 10^{-1}$ mA cm^{-2} (2.7 $\times 10^{0}$ mA cm^{-2} with the Tafel slope of 30 mV dec^{-1} for Pt as a reference), respectively. At the overpotential of 61 mV, the current density reaches 20 mA/cm^{-2} when FeP is employed as the catalyst. In contrast, WP and Ni_2P seem to be inferior to the rest, with the exchange current density in the order of 10^{-2} mA cm^{-2}, albeit the particles size of WP is only 3 nm [29].

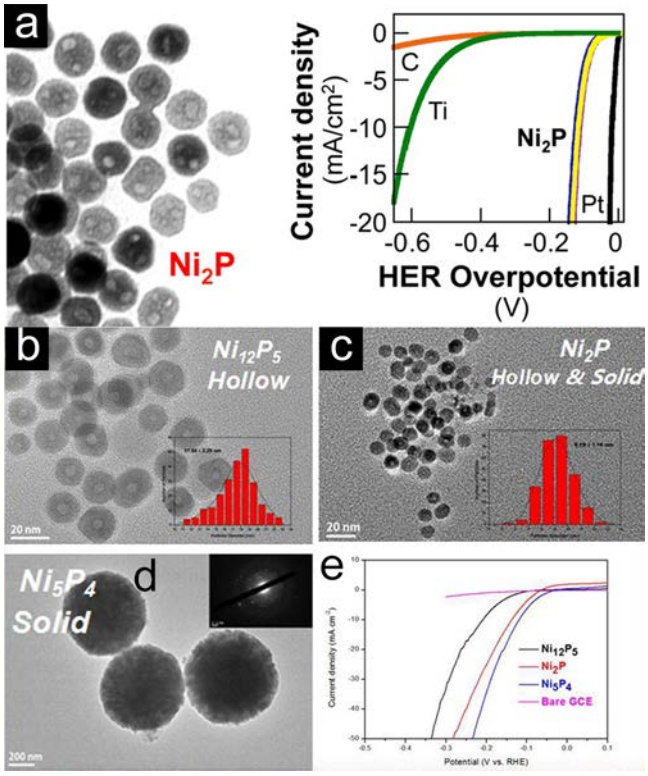

Figure 3 (a) Mono-dispersed Ni_2P nanoparticle and its polarization curve in 0.5 M H_2SO_4. Reproduced with permission.[11c] Copyright 2013, American Chemical Society; (b), (c), (d) TEM images of $Ni_{12}P_5$, Ni_2P, Ni_5P_4 respectively; (e) polarization curves of nickel phosphides ($Ni_{12}P_5$, Ni_2P, Ni_5P_4). Reproduced with permission.[34] Copyright 2015, Royal Society of Chemistry.

It is noteworthy that phosphide is not constrained by stacked loading on the electrode, and this is supported by the fact that increasing mass loading (from 0.9 mg /cm^{-2} to 2 mg cm^{-2}) leads to higher performance in the case study of CoP [27a], unlike MoS_2 that is limited by slow electron transfer among layers [5]. Interestingly, through the same synthetic method (*i.e.*, TOP route), it results in crystal forms for Ni_2P, CoP and FeP, while amorphous for MoP and WP because a higher temperature is needed for crystalline MoP and WP. However, annealing at high temperature should be avoided (> 500 ºC), as high temperature causes severe sintering, which only results in the

formation of bulk phase and degraded performance. By adopting the similar approach, *i.e.,* organic phosphine as the P source, Zhang et al. reported metal-rich phosphides for HER – Co_2P [31] and $Ni_{12}P_5$ [18b]. In comparison, metal-rich phosphides do not exhibit notably better performance than the previously reported CoP [27a] and Ni_2P [11c] or are even inferior when the overpotentials at 10 mA cm^{-2} and 20 mA cm^{-2} are compared (*e.g.*, 167 mV for Co_2P *vs.* 95 mV for CoP at 20 mA cm^{-2}), but achieve better stability in accelerated degradation test both in acidic and alkaline media for Co_2P. Given that Co_2P is in the form of nanorods, ~110 nm in length (*vs.* 9 nm particle for CoP), larger size could explain the compromised activity while the milder aggregation because of larger particle size could explain the better stability obtained in both acidic and alkaline media. A more detailed study is conducted by Schaak et al. [32] by directly comparing Co_2P with its morphological equivalent CoP that is prepared in the form of pseudospherical particles with the same particle size and particle-size distribution. Attention is drawn to the impact of stoichiometry of phosphide on its activity, *i.e.*, metal-rich *vs.* phosphorous-rich. Theoretical studies indicate that the stoichiometry of metal to phosphorus is a key concern to the activity for HER, where positive charged moiety of metal performs as hydride acceptor whilst negative charged moiety of phosphorus performs as proton acceptor; it is hypothesized that they work cooperatively for delivering molecular H_2 [31, 33]. However, experimental works implicate that higher content of phosphorus would outperform that of lower content. This is manifested on the comparative study of Co_2P and CoP where on low-index surfaces, more P atoms are exposed in CoP than that of Co_2P [32]. Another study of phase-dependent catalytic activity of nickel phosphides, including $Ni_{12}P_5$, Ni_2P and Ni_5P_4 by Pan et al. [34] also gives highlight to phosphorus, and suggests that phosphide with higher P content exhibits higher

performance, following $Ni_{12}P_5$ (29%) < Ni_2P (33%) < Ni_5P_4 (44%) (Figure 3e). When the particle size of Ni_2P and Ni_5P_4 shown in Figure 3c and 3d is taken into account, the advantage of P-rich nature would be more distinct. This enhanced effect is corroborated in the study of Ni_5P_4 by Laursen et al. [35], where micro-sized Ni_5P_4 exhibit not only higher activity, but also better stability in both acidic and alkaline media than Ni_2P. Emphasis is also given to phosphorus by Laursen et al. that firstly it is due to the basicity of P (enhanced proton bonding), and secondly phosphorus causes the contraction of Ni-Ni bond length in Ni_3 cluster that eases the first electron transfer process, and increases the second hydrogen affinity [35]. Note that the P-rich Ni_5P_4 can be realized by changing the molar ratio of P to metal. TOP route is applicable to the synthesis of various phosphides, and can provide a benchmark for the comparative studies across different phosphides, enlightening new designs of novel catalysts.

3.2. Inorganic phosphate

TOP route has enabled a size-controllable synthesis of phosphides in well-defined nanostructure that is a key attribute to guarantee a superb activity of HER. But, TOP route, apart from its sophisticated process that is an obstacle for scale-up production, involves organic phosphine that is highly toxic and can be pyrophoric in contact of leaked air. A facile and safer route is to use inorganic phosphorus – phosphate. Phosphide synthesis *via* reduction of phosphate has a long history, and becomes well known after it was used for hydrotreating process by Oyama et al. [36]. Because of the strong bond of P-O, breaking P-O and forming metal-phosphorus bond can only occur at high temperature (above 773 K for MoP). Nevertheless, this process can be facilitated by the formation of metal particles that enhances the adsorption of H on metal, spills over to phosphate, leading to the reduction of phosphate to phosphide

[21b]. Due to sintering at high temperature, phosphides *via* phosphate route usually results in bulk form with large crystal size (> 500 nm in the case of FeP sintered at 700 °C [37]). For hydrogen evolution reaction, our investigation of MoP for performing HER reveals that MoP even in bulk form (Figure 4a) has achieved a high performance in both acidic and alkaline media [17] as shown in Figure 4b, and outperforms the under-phosphorized Mo_3P and metal Mo (overpotential of 135 mV for MoP *vs.* 500 mV for Mo_3P and Mo at 10 mA cm^{-2} without i*R* correction). The exchange current density as one of the metrics for activity is found to be 3.4×10^{-2} mA cm^{-2}, at least two orders of magnitude higher than MoS_2 [7c]. The high activity of MoP is also confirmed by another independent study (Figure 4c and 4d) [38], although the morphology is different, possibly due to different scenarios of annealing. In addition, the stability through phosphate route is favorable compared to that *via* TOP route due to a better crystallinity. For example, bulk MoP performs HER stably in acidic medium for 40 h, and preserves 60 % of its initial activity in 1 M KOH after 40 h [17], whereas the cathodic current of HER fades quickly when Ni_2P is applied in alkaline medium [11c], and amorphous MoP is found to decay slightly in an accelerated degradation test in 0.5 M H_2SO_4 [28].

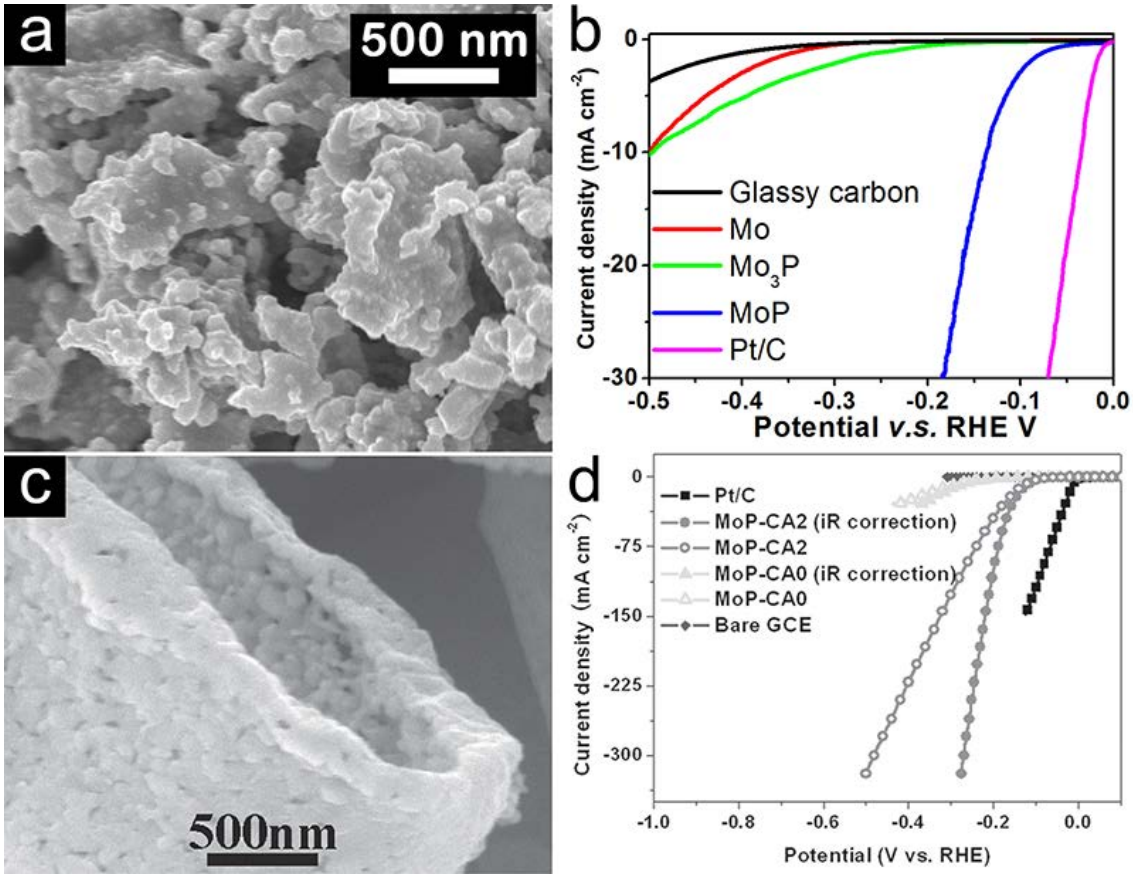

Figure 4 (a) SEM image of bulk MoP; (b) linear polarization of Mo, Mo_3P and MoP of (a) in 0.5 M H_2SO_4; Reproduced with permission.[17]. Copyright 2014, Royal Society of Chemistry; (c) Interconnected MoP particle assembly; (d) polarization curve of MoP in (c). Reproduced with permission.[38]. Copyright 2014, Wiley.

The high activity of MoP towards HER is also ascribed to its overall high electrical conductivity, suggested by Sun et al. [38]. A well interconnected network of MoP is reported to have a substantial higher conductivity (up to 149.2 S cm^{-1}) than MoS_2 (10^{-8} S cm^{-1} [39] to 0.1 S cm^{-1} [40]). We hypothesize that it would be particularly so for metal-rich ones, *e.g.* Ni_2P. Even for phosphorus rich phosphide, high conductivity is maintained. For example, WP_2 and Ni_5P_4 still possess a high conductivity of 55 S cm^{-1} [41] and 1587.3 S cm^{-1} [35] (calculated from its resistivity, 6.3 μΩ·m), respectively. The high conductivity would unequivocally contribute to the enhanced charge transfer

process. To date, no paper has reported a highly active phosphide that is layer-structured, and this could be a fortune since non-layered structured excludes the possible sluggish charge transfer among layers that makes MoS_2 suffer.

HDS involves a detachment of S from organics and deposition on catalyst. The increasing performance with time when phosphide is applied is correlated with the deposited S on the surface for HDS [42]. Given a similar process of HER to that of HDS and S-edge as a well-known active site in MoS_2 for HER, metal phosphosulfide could be an advanced catalyst to phosphide. This is verified by Jaramillo et al. [43]. Subjected to a post-sulfidation process, MoP is converted to MoP|S at 400 °C in the presence of 10% H_2S/90% H_2. The resulting MoP|S is formed in the same crystal phase as MoP (Figure 5A and 5B) with unchanged morphology. The post-sulfidation only enables a reconstruction of under-coordinated S on the surface of MoP at a depth of 10 nanometers, but brings a profoundly enhanced performance shown in Figure 5d and 5e. To drive 10 mA cm^{-2} in 0.5 M H_2SO_4, it only requires an overpotential of 86 mV for MoP|S compared to 117 mV for MoP at the mass loading of 1 mg cm^{-2}. Increased catalyst loading to 3 mg cm^{-2} gives a superior performance – overpotential of 64 mV at the current density of 10 mA cm^{-2}. This phenomenon coincides with that of CoP [27a], and has implicated a high conductivity of phosphides. TOF calculation also pinpoints the benefit of adding sulfur, 0.75 s^{-1} for MoP|S *vs.* 0.19 s^{-1} for MoP at the overpotential of 150 mV. More importantly, the post-sulfidation that embedded S on the surface promotes the stability of MoP|S compared to MoP, as evidenced by both the accelerated stability test in acid and the resistance to the surface oxidation in air. Figure 5c shows the XPS profile of the MoP and MoP|S, where the P 2p pattern shows the absence of the peak at the region of high binding energy, indicating a suppressed oxidation by the absence of PO_4^{3-} peak. Given this, sulfidation does

provide a means to improve the durability of phosphide, and complement a highly active anionic moiety – S site through reconstructing the surface. Note that the role of S in MoP|S is not fully understood at current stage, and further study is needed to unveil its structure, and the local environment that the dual anions are in.

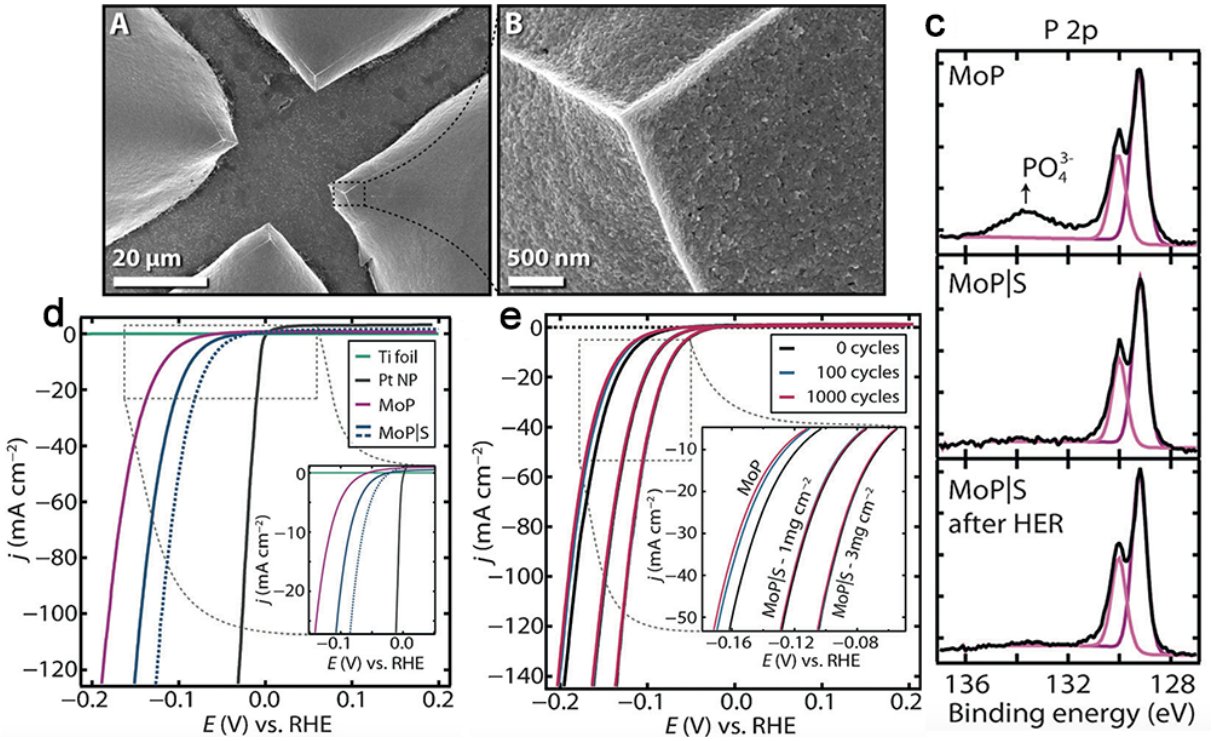

Figure 5 (A, B) Morphology of MoP on Ti foil; (c) XPS profile of P 2p for MoP, MoP|S, and MoP|S after HER; (d) linear polarization curved of MoP and MoP|S in acid; (e) stability test of MoP and MoP|S. Reproduced with permission.[43] Copyright 2014, Wiley.

3.3. On-site PH_3 from hypophosphite

Besides the two methods aforementioned, another facile route for phosphide synthesis is through the decomposition of hypophosphite [44]. A series of phosphides, *e.g.*, Ni_2P, Cu_3P, MoP and InP *etc*., can be realized *via* a physical mixture of metal salt and hypophosphite [45], or impregnation of hypophosphite solution onto metal oxide, followed by post-annealing at the temperature of ~300 °C under protective gas flow.

A modified method is through a chemical vapor deposition resembled route, where metal source is mounted separately in the downstream, reduced, and phosphidated by the on-site generated PH_3 [44] from the disproportionation of hypophosphite in the upstream. We term it hypophosphite route. Compared to TOP route, hypophosphite route enables wider options of metal precursors, *i.e.* higher flexibility, and the production of phosphide is more straightforward, free of sophisticated steps. Here, the high flexibility lies in the 'topotactic' reaction in the hypophosphite route [46], that is, the morphology of metal precursor is well preserved, which provides a facile means to synthesize nano-structured phosphides. For example, self-supported CoP nanowire arrays can be obtained from pseudomorphic transformation of Co(OH)F/carbon cloth (CC) that is realized *via* hydrothermal method. Figure 6b and 6c show the preserved nanowire structure of CoP/CC from Co(OH)F/CC that undergoes a mild phosphidation at 300 °C for 60 min. At the catalyst loading of 0.92 mg cm^{-2}, the overpotential of 115 mV drives a current density of 10 mA cm^{-2} in 1 M KOH, and in acid, the Tafel slope is determined as 51 mV dec^{-1}. TOF calculation shows that CoP/CC nanowire arrays need only 75 mV to attain 0.725 s^{-1} [47], closer to Pt (~ zero overpotential) than defect-rich MoS_2 (300 mV). In this sense, the as-grown CoP nanowires on carbon cloth enable an efficient means for hydrogen production both in acidic and alkaline media. What is more important is that the direct growth of the precursor of phosphides on Ti foil or carbon cloth and its post-phosphidation makes a better mechanical adhesion of the catalyst to the substrate [48], thus leading to a facilitated charge transfer compared to the traditional catalyst post-transferred on the electrode [48-49] (Figure 6d and 6e). For instance, to drive 2 mA cm^{-2}, the overpotential is only 26 mV for FeP nanowire array (NA)/Ti (direct growth on Ti) *vs.* 225 mV for FeP nanowire (NW)/Ti (immobilized by Nafion solution) shown in Figure 6f. A

similar structure of FeP directly grown on Ti plate is reported by Li et al. [50], and the high performance is also confirmed. At an overpotential of 85 mV and with an even lower catalyst loading of 0.6 mg cm^{-2}, current density reaches 10 mA cm^{-2} and TOF is 2.58 s^{-1}. The direct growth of metal salt (the precursor of phosphide) can be realized *via* electro-deposition or hydrothermal synthesis [50-51]. Given the significance of the strong interaction between the electro-catalyst and the substrate/current collector, strategies to enhance the interaction could be promising and impactful. Sintering at high temperature would possibly enable a better contact of the catalyst and the substrate. For example, by dip-coating a mixed solution of Fe precursor with polyvinylpyrrolidone (PVP) in N,N-dimethylformamide (DMF) on carbon cloth and high-temperature sintering at 600 °C, the as-obtained Fe_3O_4 is found in a close contact with carbon cloth; a subsequent phosphidation transforms Fe_3O_4 to FeP/CC (iron phosphide nanoparticles deposited on carbon cloth) with an enhanced catalyst-substrate (carbon cloth) interaction. The performance is remarkably high in catalyzing HER, almost similar to Pt/C [52], with the Tafel slope of 32 mV dec^{-1}, 20 mA cm^{-2} at an overpotential of 54 mV.

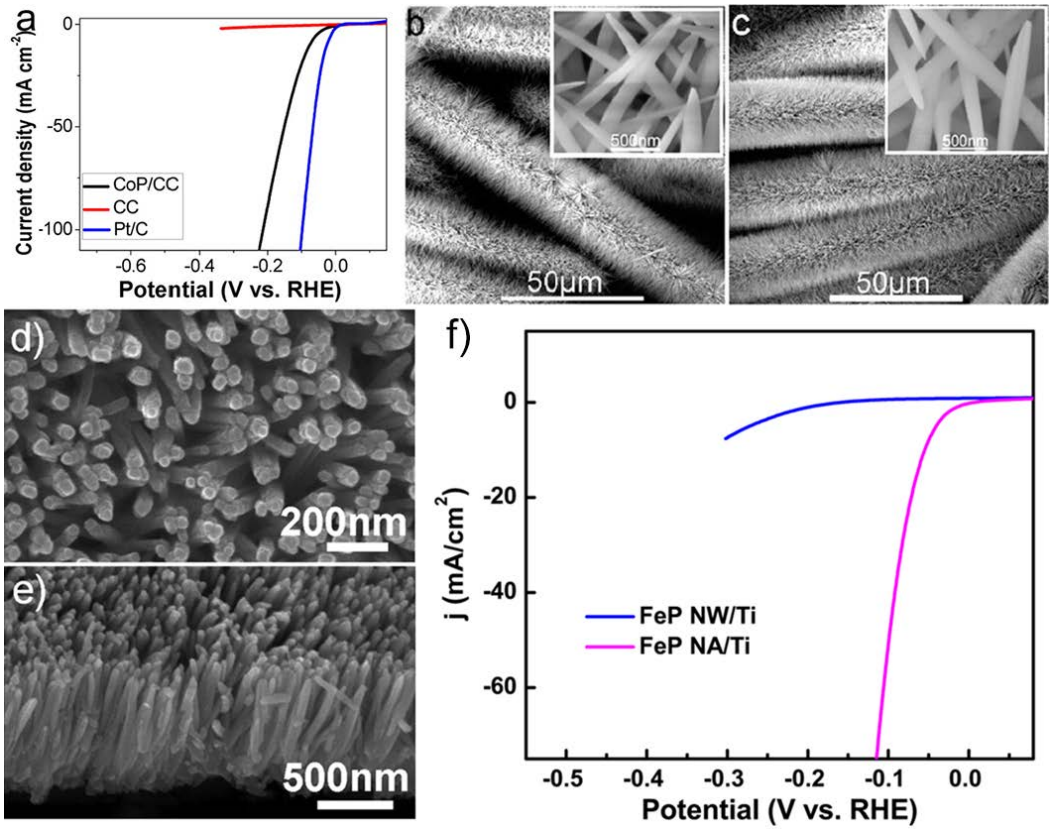

Figure 6 (a) polarization curves of CoP grown carbon cloth (CoP/CC), blank carbon cloth (CC) and Pt/C; SEM image of (b) Co(OH)F and (c) CoP grown on carbon cloth. Reproduced with the permission.[47] Copyright 2014, American Chemical Society; (d, e) SEM images of FeP grown on Ti foil; (f) linear polarization curves of FeP nanowire array/Ti and FeP nanowire/Ti. Reproduced with permission.[48] Copyright 2014, Wiley.

The direct-growth approach also applies to CoP [51a] and Ni_2P [51b] *via* an electrochemical deposition in their respective nitrate solutions although the electro-deposition results in nanosheets for CoP, but compact film structure consisting of nanoparticles for Ni_2P. At the same mass loading, CoP nanosheet array outperforms Ni_2P film, and this indicates that the activity towards HER is highly correlated with the structure. The higher aspect ratio of nanosheets CoP would possibly provide more accessible sites for protons and faster mass diffusion than the compact film. The

performance-structure correlation is fully manifested in the study of Cu_3P [18a] and CoP [53] as catalysts for HER, where Cu_3P NW/CF (nanowire grown on copper foam) outperforms Cu_3P MF/CF (microparticles coated copper foam) [18a]; the CoP nanotubes (CoP NTs) outperforms CoP nanoparticles (CoP NPs) [53]. Adopting the post-phosphidation approach, uniformly distributed nano-sized phosphide can be obtained by incorporation of carbon materials, *e.g.*, CoP decorated carbon nanotube [54] (Figure 7a), CoP on rGO [55]/ mesoporous carbon [56], Fe-doped Ni_2P sandwiched by quasi-graphene [57]. Emphasis is given to the abundant active sites from the supported nano-sized phosphide compared to its supportless counterpart. As shown in Figure 7b, a two-step synthesis of cobalt phosphide enables a highly distributed CoP nanoparticles on various carbon substrates, which provides large amount of active sites for HER (CoP/RGO in Figure 7c). High electrical conductivity of the carbon materials also ensures efficient electron transfer.

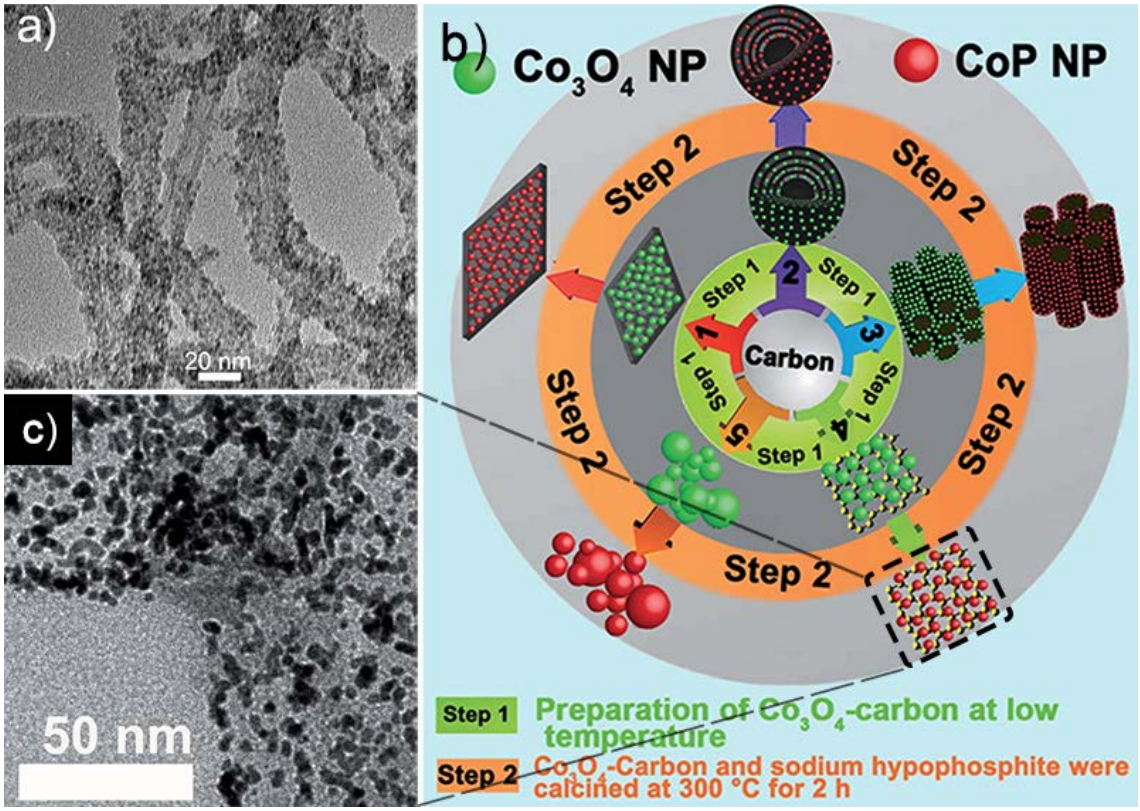

Figure 7 (a) TEM image of CoP on carbon nanotube. Reproduced with permission.[54] Copyright 2014, Wiley; (b) schematic illustration of a two-step synthesis of CoP on various carbon substrates, with CoP/RGO in (c). Reproduced with permission.[56] Copyright 2015, Royal Society of Chemistry.

Table I Summary of the HER performance of phosphides synthesized through TOP route, phosphate route and hypophosphite route.

	Catalyst	Electrolyte	Exchange current density (10^{-2} mA cm^{-2})	Tafel slope (mV dec^{-1})	Turnover frequency (TOF, s^{-1}@ mV)	Over-potential at the corresponding *j* (mV@ mA cm^{-2})
TOP route	Nanostructured Ni_2P/Ti [11c]	0.5M H_2SO_4	3.3	46	0.015@100 0.5 @200	130@20 180@100
	Nanostructured CoP/Ti [27a]	0.5M H_2SO_4	14	50	0.038-0.046@100	95@20
	Amorphous MoP/Ti [28]	0.5M H_2SO_4	12	45	—	90@10 105@20
	Amorphous WP/Ti [29]	0.5M H_2SO_4	4.5	54	—	120@10 140@20
	Nanostructured FeP/Ti [30]	0.5M H_2SO_4	43	37	0.277@100	50@10
	Co_2P nanorod [31]	—	—	71 or 52	0.725@143 in 0.5M H_2SO_4	167@20 in 0.5M H_2SO_4 171@20 in 1 M KOH
	$Ni_{12}P_5$ nanoparticle [18b]	0.5M H_2SO_4	—	63	—	137@10 175@20
	Nanostructured Co_2P/Ti [32]	0.5M H_2SO_4	—	45	—	95@10 109@20
	Nanocrystalline Ni_5P_4 [35]	—	—	33	3.5@100, 9.8@200 in 1M H_2SO_4 0.79@100, 2.9@200 in 1M NaOH	23@10, 62@100 in 1M H_2SO_4 49@10, 202@100 in 1M NaOH
	Mono-dispersed [34] $Ni_{12}P_5$	0.5M H_2SO_4	—	75	—	208@10
	Mono-dispersed [34] Ni_2P			49		137@10
	Mono-dispersed [34] Ni_5P_4			42		118@10
	Highly Branched CoP/Ti [27b]	0.5M H_2SO_4	—	48	0.019@100	117@20
	MoP [17]	—	3.4	54 in 0.5M H_2SO_4	—	180@30

Phosphate route			4.6	48 in 1M KOH		—
	Interconnected MoP [38]	0.5M H_2SO_4	8.6	54	—	125@10 200@100
	WP_2 sub-microparticles [41]	0.5M H_2SO_4	1.7	57	—	161@10 294@100
	Molybdenum Phosphosulfide MoP|S [43]	0.5M H_2SO_4	20 (1mg cm^{-2})	50	0.12@100, 0.75@150	90@10 with 1mg cm^{-2} mas loading
			57 (3mg cm^{-2})			64@10, 125@100 with 3mg cm^{-2} mass loading
	MoP[a] microparticles [58]	—	1	50	—	150@10 in 0.5M H_2SO_4
						330@10 in 0.2M borate buffer solution
						190@10 in 1M KOH
	MoP particles [59]	0.5M H_2SO_4	0.42	60	0.048@100	246@10
Hypophosphite route	Ni_2P nanoparticles [45]	—	—	87	—	140@20 in 1M H_2SO_4
				100		250@20 in 1M KOH
	CoP nanotube(CoP NT) [53]	0.5M H_2SO_4	—	60	1@106	72@2, 129@10 for CoP NT
	CoP nanoparticles (CoP NP) [53]			82	1@172	200@2, 297@10 for CoP NP
	3D nanoporous CoP/Ti [46]	0.5M H_2SO_4	—	65	—	95@20 220@100
	CoP NWs [49b]	0.5M H_2SO_4	16	54	—	110@10
	CoP NSs [49b]		3.2	61		160@10
	CoP NPs [49b]		5.4	87		221@10
	FeP nanowire array/Ti [48]	0.5M H_2SO_4	42	38	—	55@10, 127@100
	Amorphous W doped nickel phosphide (a-WNiP) [60]	0.5M H_2SO_4	4.4	39	0.725@100	110@20
	CoP nanoparticle film [61]	0.5M H_2SO_4	—	70	—	48@10, 190@100
	FeP nanorod array [51c]	—	50	45 in 0.5M H_2SO_4	—	58@10 in 0.5M H_2SO_4
			—	71 in 1M PBS		202@10 in 1M PBS

Hypophosphite route			—	146 in 1 M KOH		218@10 in 1M KOH
	CoP/CNT [54]	0.5M H_2SO_4	13	54	—	70@2, 122@10
	FeP naonrod array/Ti [50]	0.5M H_2SO_4	—	60	2.58@85	85@10, 183@240
	WP nanorod array [62]	0.5M H_2SO_4	29	69	—	130@10, 230@100
	CoP nanosheet array/Ti [51a]	0.5M H_2SO_4	—	43	—	90@10, 146@100
	Ni_2P nanoparticle film/Ti [51b]	1M H_2SO_4	—	60	0.725@205	138@20, 188@100
	Nanoporous Cobalt Phosphide Nanowire Arrays [47]	—	28.8	51	0.725@75, 4@240 in 0.5M H_2SO_4	67@10, 100@20, 204@100 in 0.5M H_2SO_4
			—	93		65@2 in 1M PBS
			—	129		209@10 in 1M KOH
	Cu_3P Nanowire Arrays [18a]	0.5M H_2SO_4	18	67	—	143@10
	FeP Nanoparticles Film on carbon cloth [52]	0.5M H_2SO_4	59	32	—	54@20, 108@100
	Fe/GSs [49c]	0.5M H_2SO_4	12	50	—	123@10
	MoP nanosheets/carbon flakes [49a]	0.5M H_2SO_4	—	56	—	200@10
	WP_2 nanorods [63]	0.5M H_2SO_4	1.3	52	~6.58@200	101@2, 148@10
	CoP-OMC [56]	0.5M H_2SO_4	16.1	56.7	2.7@200 for CoP-OMC	112.18@10
	CoP-RGO [56]		5.7	70.2		156.87@10
	CoP-MPC [56]		7.4	69.8		141.73@10
	CoP-MCV [56]		9.1	63.1		134.34@10

[a]: the MoP is commercially purchased.

The performance of the various catalysts prepared by TOP, phosphate and hypophosphite route is summarized in Table I. It can be seen that the activities vary greatly among different catalysts. Unfortunately, the origin of the activity and the so-called synergistic effect between the metal moiety and phosphorus moiety are not fully understood and still remain at the stage of theoretical study. It is only suggested that positive charged metal behaves as a hydride acceptor whilst negative charged phosphorus behaves as a proton acceptor [18, 33]. As for the exact mechanism on the hydrogen evolution including adsorption of H, diffusion and desorption of molecular H_2 on phosphide, few work has presented a comprehensive study. Emphasis has been given on both metal part, as in W doped nickel phosphide [60], and phosphorus part, as in anion-proliferated phosphosulfide [43]. It seems that a balanced-stoichiometry composite is preferred instead of seeking for either metal-rich or phosphorus-rich since WP_2 does not show pronounced advantages over WP [41, 62-63].

4. Other emerging routes

Besides these three routes, phosphorus in the forms of elemental phosphorus, such as red/yellow phosphorus [62, 64], and phosphorous acid (H_3PO_3) [65] has also been successfully employed for the synthesis of phosphide. For example, Sun et al. [62] reported a tungsten phosphide by using red phosphorus as the phosphorus source at 800 °C; Yang et al. [64b] reported a phosphorus-rich iron phosphide by red phosphorus. The performance reported is inferior to that via hypophosphite route, which we believe is due to the long-term calcination at high temperature. Unfortunately, neither of the two studies highlighted the advantage of using element phosphorus. In a sense, element phosphorus could provide an independent phosphorus source for phosphidation; and by varying the synthesis conditions (phosphorus molar ratio, temperature *etc*.), both metal-rich and phosphorus-rich phosphides could be obtained

with high yield. Given this, single element phosphorus source would still be promising if particle aggregation at high temperature can be circumvented. Impactful future work is needed to tackle this issue.

Another method to introduce phosphorus is through electrochemical reduction of phosphorous acid in the presence of nickel/cobalt [65-66]. The experiment is conducted in a mixed solution of nickel/cobalt sulfate and phosphorous acid with some other additives. Here, the phosphorous acid can be replaced by hypophosphite in acidic condition. The as-obtained product is deemed as a metal-phosphorus alloy in the case of nickel-phosphorus [65a], and the performance of nickel-P towards HER in acid has not yet been reported. Not until recently, Cobalt-phosphorus film was found to be able to catalyze HER in a remarkably high efficiency by Sun et al. [66] in alkaline. Given the high cobalt content (Co/P ≈ 6.98) and the formation at room temperature [66], the structure of Co-phosphorus film has yet to be unveiled. However, the electrochemical reduction of high-valence phosphorus enables an alternative way to incorporate phosphorus at room temperature, and provides a potential solution to avoid calcination at high temperature.

5. Conclusions and Perspectives

5.1. Summary

In this review article, we have summarized the recent development of non-noble metal catalyst for hydrogen evolution reaction with focus on phosphides based on the synthetic methods. Through a comprehensive survey of phosphide synthesis, *i.e.*, TOP, phosphate route and hypophosphite route, we present the pros and cons for each approach. In a nutshell, phosphides as a newly recognized catalyst for HER exhibit advantageous performance over the state-of-the-art molybdenum sulfide, and the highlighted advantages lie in the features: (1) low onset potential, nearly zero for FeP/CC [52] *vs.* 150 ~ 200 mV for that of MoS_2, and high current density at low overpotential, 10 mA cm^{-2} at an overpotential of 54 mV; (2) transitional metal phosphides exhibit metallic properties, *i.e.*, high electrical conductivity [18a], unlike MoS_2, which is conductive only with thin-layer configuration [5] due to its sluggish electron transfer among layers; (3) Phosphides are free from the constraint of fabrication of layered structure or nanostructure required to ensure superb performance for MoS_2. Herein, bulk MoP is found to be very active towards HER. Out of intensive focus on the methodologies since the first report of Ni_2P for eletrocatalysis HER, the well-established TOP, phosphate and hypophosphite routes have realized a series of the highly active electro-catalysts for HER in acid, but the understanding of the active sites is still falling behind. In this review article, based on limited published results on theoretical calculations, we have provided a correlative interpretation of the experimental metrics – Tafel plot & exchange current density with Gibbs free energy ($\Delta G_{cat\text{-}H}$) from theoretical prediction of hydrogen ad/desorption on the catalyst. It is proposed that in phosphide, the negative charged P site and positive charged metal site could be working synergistically for delivering

molecular hydrogen instead of being solely dependent on phosphorus site. More detailed description on the role of active sites on individual phosphide requires in-depth study of the hydrogen adsorption, diffusion, and combination on specific facet. Due to the complexity of the geometry of the surfaces (the kinks, twists & bonding strength on the active sites) as well the varieties of crystal structures of phosphides, future works are warranted to bridge the gap of theoretical prediction and experimental observation.

5.2. Challenges and Future perspectives

Despite the outstanding performances that phosphides have gone beyond the state-of-the-art non-noble-metal catalyst – sulfides [67], challenges still co-exist for this new-generation HER electro-catalysts. As revealed by XPS analysis, surface oxidation occurs under ambient condition, resulting in the formation of P (V) and metal oxide (high-valence state) in almost all the phosphides. This as-formed non-active oxide would clearly block the access of proton to the active site and lower the conductivity, which will cause fast-degraded performance. Note that the stability/durability of the investigated catalyst is evaluated by potentiostatic/galvanostatic technique, where the cathodic potential in a reducing environment (bubbling molecular hydrogen) may have masked the deficiency of phosphides being unstable even in ambient air. This could be a direct consequence of the extremely highly active negative-charged P site. In contrast, the activity of MoS_2 for HER is maintained upon six months' exposure in air [68]. Surface engineering would provide a good solution to the unstable P site; the instability on the surface could be caused by the under-coordinated P site that is also the origin of the high activity towards HER. Jaramillo et al. [43] have built sulfur anions into MoP, which greatly suppresses the oxidation on the surface. Continued work are being called forth to apply to other phosphides, and uncover alternative

anions that not only improve the stability in ambient air, but also multiply the active sites, leading to enhanced activities.

In hindsight, the enhanced activity of phosphides compared to molybdenum disulfide is firstly owing to the high conductivity as we have highlighted in the summary part. To rival Pt, research focus in future is still to be placed on the improvement of the activity. In this perspective, material doping/defect engineering that allows materials modulation in the lattice level, mesopore-structured material synthesis/porosity-optimization are viable, and can be the key factors that contribute to the advancement of phosphide material for electro-catalytic HER. For instance, W doping [60], Fe-doping phosphide [57] have been initiated; metal-organic framework (MOF) derived mesoporous phosphide [69] has showcased. The resultant phosphides with those characteristics – high conductivity, optimum porosity with high surface area in a well-defined structure, multiplied active sites, good crystallinity that ensures high corrosion-resistance, *i.e.*, high sustainability, would be favored.

The TOP, phosphate and hypophosphite routes that could provide complementary pathways to enable those characteristics thereof, have been well-established. The newly emerged routes to incorporate phosphorus – element phosphorus and electrochemical reduction are viable, and they are still at their nascent stage in terms of the application in electro-catalytic HER. All the approaches together for phosphides can be potentially used for the synthesis of a photo-catalyst for photo-catalytic hydrogen production. Due to the semi-metallic/metallic properties of phosphides, which means very narrow or zero band gap, photo-catalytic HER solely using phosphide is impractical, low efficient. Co-catalyst with semi-conductors, *e.g.*, CdS/ZnS [70] would be feasible. Surface disordering, likewise the modified band structure in black titanium oxide [71], is worth exploring. More realistically, surface

sensitization by incorporating photo-sensitizer as a light-absorber would be promising. In this regard, highly active phosphides in a good thermodynamic ad/desorption of hydrogen readily function in photo-catalysis.

With the capability of realizing a series of phosphides with controlled structure and stoichiometry (from metal-rich to phosphorus-rich) in both photo/electro-catalysis, these approaches together could provide a benchmarked platform for experimental investigation of phosphides in the origins of the high activity, clarifying the possible synergistic effect that may provide a fundamental guideline for catalyst design of the next generation and eventually enable a cost-effective, efficient hydrogen production.

Acknowledgment

This project is funded by the National Research Foundation (NRF), Prime Minister's Office, Singapore under its Campus for Research Excellence and Technological Enterprise (CREATE) programme. We also acknowledge financial support from the academic research fund AcRF tier 1 (M4011020 RG8/12 and M4011253 RG 7/14) Ministry of Education, Singapore.

References

[1] T. F. Jaramillo, K. P. Jørgensen, J. Bonde, J. H. Nielsen, S. Horch, I. Chorkendorff, *Science* **2007**, 317, 100.

[2] H. Tributsch, J. C. Bennett, *J. electroanal. chem. interfacial electrochem.* **1977**, 81, 97.

[3] C. G. Morales-Guio, X. Hu, *Acc. Chem. Res.* **2014**, 47, 2671.

[4] Y. Yan, B. Xia, Z. Xu, X. Wang, *ACS Catal.* **2014**, 4, 1693.

[5] Y. Yu, S.-Y. Huang, Y. Li, S. N. Steinmann, W. Yang, L. Cao, *Nano Lett.* **2014**, 14, 553.

[6] a) M. A. Lukowski, A. S. Daniel, F. Meng, A. Forticaux, L. Li, S. Jin, *J. Am. Chem. Soc.* **2013**, 135, 10274. ; b) M. S. Faber, S. Jin, *Energy Environ. Sci.* **2014**, 7, 3519.

[7] a) Z. Wu, B. Fang, A. Bonakdarpour, A. Sun, D. P. Wilkinson, D. Wang, *Appl. Catal. B Environ.* **2012**, 125, 59. ; b) L. Cheng, W. Huang, Q. Gong, C. Liu, Z. Liu, Y. Li, H. Dai, *Angew. Chem. Int. Ed.* **2014**, 53, 7860. ; c) D. Merki, X. Hu, *Energy Environ. Sci.* **2011**, 4, 3878.

[8] a) D. Kong, H. Wang, J. J. Cha, M. Pasta, K. J. Koski, J. Yao, Y. Cui, *Nano Lett.* **2013**, 13, 1341. ; b) H. Wang, D. Kong, P. Johanes, J. J. Cha, G. Zheng, K. Yan, N. Liu, Y. Cui, *Nano Lett.* **2013**, 13, 3426. ; c) D. Kong, H. Wang, Z. Lu, Y. Cui, *J. Am. Chem. Soc.* **2014**, 136, 4897.

[9] D. Kong, J. J. Cha, H. Wang, H. R. Lee, Y. Cui, *Energy Environ. Sci.* **2013**, 6, 3553.

[10] a) A. B. Laursen, S. Kegnaes, S. Dahl, I. Chorkendorff, *Energy Environ. Sci.* **2012**, 5, 5577. ; b) M. Wang, L. Chen, L. Sun, *Energy Environ. Sci.* **2012**, 5, 6763. ; c) J. R. Mckone, S. C. Marinescu, B. S. Brunschwig, J. R. Winkler, H. B. Gray, *Chem. Sci.* **2014**, 5, 865.

[11] a) P. Liu, J. A. Rodriguez, T. Asakura, J. Gomes, K. Nakamura, *The Journal of Physical Chemistry B* **2005**, 109, 4575. ; b) S. T. Oyama, T. Gott, H. Y. Zhao, Y. K. Lee, *Catal. Today* **2009**, 143, 94. ; c) E. J. Popczun, J. R. Mckone, C. G. Read, A. J. Biacchi, A. M. Wiltrout, N. S. Lewis, R. E. Schaak, *J. Am. Chem. Soc.* **2013**, 135, 9267.

[12] a) J. K. Nørskov, T. Bligaard, A. Logadottir, J. R. Kitchin, J. G. Chen, S. Pandelov, U. Stimming, *J. Electrochem. Soc.* **2006**, 153, L33. ; b) J. K. Nørskov, T. Bligaard, A. Logadottir, J. R. Kitchin, J. G. Chen, S. Pandelov, U. Stimming, *J. Electrochem. Soc.* **2005**, 152, J23. ; c) Y. Zheng, Y. Jiao, M. Jaroniec, S. Z. Qiao, *Angew. Chem. Int. Ed.* **2014**, 54, 52. ; d) B. Hinnemann, P. G. Moses, J. Bonde, K. P. Jørgensen, J. H. Nielsen, S. Horch, I. Chorkendorff, J. K. Nørskov, *J. Am. Chem. Soc.* **2005**, 127, 5308.

[13] a) P. Liu, J. Rodriguez, *Catal. Lett.* **2003**, 91, 247. ; b) R. R. Chianelli, G. Berhault, P. Raybaud, S. Kasztelan, J. Hafner, H. Toulhoat, *Appl. Catal. A Gen.* **2002**, 227, 83.

[14] P. Clark, X. Wang, S. T. Oyama, *J. Catal.* **2002**, 207, 256.

[15] T. Todorova, R. Prins, T. Weber, *J. Catal.* **2005**, 236, 190.

[16] a) S. T. Oyama, *J. Catal.* **2003**, 216, 343. ; b) D. C. Phillips, S. J. Sawhill, R. Self, M. E. Bussell, *J. Catal.* **2002**, 207, 266. ; c) C. Stinner, R. Prins, T. Weber, *J. Catal.* **2001**, 202, 187.

[17] P. Xiao, M. Alam Sk, L. Thia, X. Ge, R. J. Lim, J.-Y. Wang, K. H. Lim, X. Wang, *Energy Environ. Sci.* **2014**, 7, 2624.

[18] a) J. Tian, Q. Liu, N. Cheng, A. M. Asiri, X. Sun, *Angew. Chem. Int. Ed.* **2014**, 53, 9577. ; b) Z. Huang, Z. Chen, Z. Chen, C. Lv, H. Meng, C. Zhang, *ACS Nano* **2014**, 8, 8121.
[19] J.-S. Moon, J.-H. Jang, E.-G. Kim, Y.-H. Chung, S. J. Yoo, Y.-K. Lee, *J. Catal.* **2015**, 326, 92.
[20] M. H. Hansen, L.-A. Stern, L. Feng, J. Rossmeisl, X. Hu, *Phys. Chem. Chem. Phys.* **2015**, 17, 10823.
[21] a) S. Carenco, D. Portehault, C. Boissière, N. Mézailles, C. Sanchez, *Chem. Rev.* **2013**, 113, 7981. ; b) R. Prins, M. Bussell, *Catal. Lett.* **2012**, 142, 1413.
[22] a) S. C. Perera, G. Tsoi, L. E. Wenger, S. L. Brock, *J. Am. Chem. Soc.* **2003**, 125, 13960. ; b) K. A. Gregg, S. C. Perera, G. Lawes, S. Shinozaki, S. L. Brock, *Chem. Mater.* **2006**, 18, 879.
[23] A. E. Henkes, Y. Vasquez, R. E. Schaak, *J. Am. Chem. Soc.* **2007**, 129, 1896.
[24] E. Muthuswamy, P. R. Kharel, G. Lawes, S. L. Brock, *ACS Nano* **2009**, 3, 2383.
[25] H. Vrubel, T. Moehl, M. Gratzel, X. Hu, *Chem. Commun.* **2013**, 49, 8985.
[26] W.-F. Chen, J. T. Muckerman, E. Fujita, *Chem. Commun.* **2013**, 49, 8896.
[27] a) E. J. Popczun, C. G. Read, C. W. Roske, N. S. Lewis, R. E. Schaak, *Angew. Chem. Int. Ed.* **2014**, 53, 5427. ; b) E. J. Popczun, C. W. Roske, C. G. Read, J. C. Crompton, J. M. Mcenaney, J. F. Callejas, N. S. Lewis, R. E. Schaak, *J. Mater. Chem. A* **2015**, 3, 5420.
[28] J. M. Mcenaney, J. C. Crompton, J. F. Callejas, E. J. Popczun, A. J. Biacchi, N. S. Lewis, R. E. Schaak, *Chem. Mater.* **2014**, 26, 4826.
[29] J. Mcenaney, J. C. Crompton, J. Callejas, E. Popczun, C. Read, N. Lewis, R. Schaak, *Chem. Commun.* **2014**, 50, 11026.
[30] J. F. Callejas, J. M. Mcenaney, C. G. Read, J. C. Crompton, A. J. Biacchi, E. J. Popczun, T. R. Gordon, N. S. Lewis, R. E. Schaak, *ACS Nano* **2014**, 8, 11101.
[31] Z. Huang, Z. Chen, Z. Chen, C. Lv, M. G. Humphrey, C. Zhang, *Nano Energy* **2014**, 9, 373.
[32] J. F. Callejas, C. G. Read, E. J. Popczun, J. M. Mcenaney, R. E. Schaak, *Chem. Mater.* **2015**, 27, 3769.
[33] P. Liu, J. A. Rodriguez, *J. Am. Chem. Soc.* **2005**, 127, 14871.
[34] Y. Pan, Y. Liu, J. Zhao, K. Yang, J. Liang, D. Liu, W. Hu, D. Liu, Y. Liu, C. Liu, *J. Mater. Chem. A* **2015**, 3, 1656.
[35] A. B. Laursen, K. R. Patraju, M. J. Whitaker, M. Retuerto, T. Sarkar, N. Yao, K. V. Ramanujachary, M. Greenblatt, G. C. Dismukes, *Energy Environ. Sci.* **2015**, 8, 1027.
[36] W. Li, B. Dhandapani, S. T. Oyama, *Chem. Lett.* **1998**, 27, 207.
[37] K. L. Stamm, J. C. Garno, G.-Y. Liu, S. L. Brock, *J. Am. Chem. Soc.* **2003**, 125, 4038.
[38] Z. Xing, Q. Liu, A. M. Asiri, X. Sun, *Adv. Mater.* **2014**, 26, 5702.
[39] J. N. Coleman, M. Lotya, A. O'neill, S. D. Bergin, P. J. King, U. Khan, K. Young, A. Gaucher, S. De, R. J. Smith, I. V. Shvets, S. K. Arora, G. Stanton, H.-Y. Kim, K. Lee, G. T. Kim, G. S. Duesberg, T. Hallam, J. J. Boland, J. J. Wang, J. F. Donegan, J. C. Grunlan, G. Moriarty, A. Shmeliov, R. J. Nicholls, J. M. Perkins, E. M. Grieveson, K. Theuwissen, D. W. Mccomb, P. D. Nellist, V. Nicolosi, *Science* **2011**, 331, 568.
[40] G. Eda, H. Yamaguchi, D. Voiry, T. Fujita, M. Chen, M. Chhowalla, *Nano Lett.* **2011**, 11, 5111.
[41] Z. Xing, Q. Liu, A. M. Asiri, X. Sun, *ACS Catal.* **2014**, 5, 145.

[42] a) J. Bai, X. Li, A. J. Wang, R. Prins, Y. Wang, *J. Catal.* **2013**, 300, 197. ; b) X. Duan, Y. Teng, A. Wang, V. M. Kogan, X. Li, Y. Wang, *J. Catal.* **2009**, 261, 232.
[43] J. Kibsgaard, T. F. Jaramillo, *Angew. Chem. Int. Ed.* **2014**, 53, 14433.
[44] a) Q. X. Guan, W. Li, M. H. Zhang, K. Y. Tao, *J. Catal.* **2009**, 263, 1. ; b) Q. X. Guan, W. Li, *J. Catal.* **2010**, 271, 413.
[45] L. Feng, H. Vrubel, M. Bensimon, X. Hu, *Phys. Chem. Chem. Phys.* **2014**, 16, 5917.
[46] S. Gu, H. Du, A. M. Asiri, X. Sun, C. M. Li, *Phys. Chem. Chem. Phys.* **2014**, 16, 16909.
[47] J. Tian, Q. Liu, A. M. Asiri, X. Sun, *J. Am. Chem. Soc.* **2014**, 136, 7587.
[48] P. Jiang, Q. Liu, Y. Liang, J. Tian, A. M. Asiri, X. Sun, *Angew. Chem. Int. Ed.* **2014**, 53, 12855.
[49] a) W. Cui, Q. Liu, Z. Xing, A. M. Asiri, K. A. Alamry, X. Sun, *Appl. Catal. B Environ.* **2015**, 164, 144. ; b) P. Jiang, Q. Liu, C. Ge, W. Cui, Z. Pu, A. M. Asiri, X. Sun, *J. Mater. Chem. A* **2014**, 2, 14634. ; c) Z. Zhang, B. Lu, J. Hao, W. Yang, J. Tang, *Chem. Commun.* **2014**, 50, 11554.
[50] R. Liu, S. Gu, H. Du, A. M. Asiri, C. Li, *J. Mater. Chem. A* **2014**, 2, 17263.
[51] a) Z. Pu, Q. Liu, P. Jiang, A. M. Asiri, A. Y. Obaid, X. Sun, *Chem. Mater.* **2014**, 26, 4326. ; b) Z. Pu, Q. Liu, C. Tang, A. M. Asiri, X. Sun, *Nanoscale* **2014**, 6, 11031. ; c) Y. H. Liang, Q. Liu, A. M. Asiri, X. P. Sun, Y. L. Luo, *ACS Catal.* **2014**, 4, 4065.
[52] J. Tian, Q. Liu, Y. Liang, Z. Xing, A. M. Asiri, X. Sun, *ACS Appl. Mater. Interfaces* **2014**, 6, 20579.
[53] H. Du, Q. Liu, N. Cheng, A. M. Asiri, X. Sun, C. M. Li, *J. Mater. Chem. A* **2014**, 2, 14812.
[54] Q. Liu, J. Tian, W. Cui, P. Jiang, N. Cheng, A. M. Asiri, X. Sun, *Angew. Chem. Int. Ed.* **2014**, 53, 6710.
[55] L. B. Ma, X. P. Shen, H. Zhou, G. X. Zhu, Z. Y. Ji, K. M. Chen, *J. Mater. Chem. A* **2015**, 3, 5337.
[56] M. Li, X. Liu, Y. Xiong, X. Bo, Y. Zhang, C. Han, L. Guo, *J. Mater. Chem. A* **2015**, 3, 4255.
[57] Y. Feng, Y. Ouyang, L. Peng, H. Qiu, H. Wang, Y. Wang, *J. Mater. Chem. A* **2015**, 10.1039/C5TA01103E.
[58] T. Y. Wang, K. Z. Du, W. L. Liu, Z. W. Zhu, Y. H. Shao, M. X. Li, *J. Mater. Chem. A* **2015**, 3, 4368.
[59] X. Chen, D. Wang, Z. Wang, P. Zhou, Z. Wu, F. Jiang, *Chem. Commun.* **2014**, 50, 11683.
[60] Z. Jin, P. Li, X. Huang, G. Zeng, Y. Jin, B. Zheng, D. Xiao, *J. Mater. Chem. A* **2014**, 2, 18593.
[61] Q. Li, Z. Xing, A. M. Asiri, P. Jiang, X. Sun, *Int. J. Hydrogen Energy* **2014**, 39, 16806.
[62] Z. Pu, Q. Liu, A. M. Asiri, X. Sun, *ACS Appl. Mater. Interfaces* **2014**, 6, 21874.
[63] H. Du, S. Gu, R. Liu, C. M. Li, *J. Power Sources* **2015**, 278, 540.
[64] a) Y. Xie, H. L. Su, X. F. Qian, X. M. Liu, Y. T. Qian, *J. Solid State Chem.* **2000**, 149, 88. ; b) J. Jiang, C. Wang, J. Zhang, W. Wang, X. Zhou, B. Pan, K. Tang, J. Zuo, Q. Yang, *J. Mater. Chem. A* **2015**, 3, 499. ; c) S. Sarkar, S. Sampath, *Chem. Commun.* **2014**, 50, 7359. ; d) A. R. J. Kucernak, V. N. N. Sundaram, *J. Mater. Chem. A* **2014**, 2, 17435.

[65] a) A. Kurowski, J. W. Schultze, G. Staikov, *Electrochem. Commun.* **2002**, 4, 565. ; b) Y. Xu, X. M. Ge, B. Y. Du, C. Xu, Y. W. Wang, J. Z. Jiang, *J. Electrochem. Soc.* **2008**, 155, D731.
[66] N. Jiang, B. You, M. Sheng, Y. Sun, *Angew. Chem. Int. Ed.* **2015**, 54, 6251.
[67] X. Zou, Y. Zhang, *Chem. Soc. Rev.* **2015**, 10.1039/C4CS00448E.
[68] J. Xie, J. Zhang, S. Li, F. Grote, X. Zhang, H. Zhang, R. Wang, Y. Lei, B. Pan, Y. Xie, *J. Am. Chem. Soc.* **2013**, 135, 17881.
[69] J. Hao, W. Yang, Z. Zhang, J. Tang, *Nanoscale* **2015**, 10.1039/C5NR01955A.
[70] Z. Sun, Q. Yue, J. Li, J. Xu, H. Zheng, P. Du, *J. Mater. Chem. A* **2015**, 3, 10243.
[71] X. Chen, L. Liu, P. Y. Yu, S. S. Mao, *Science* **2011**, 331, 746.

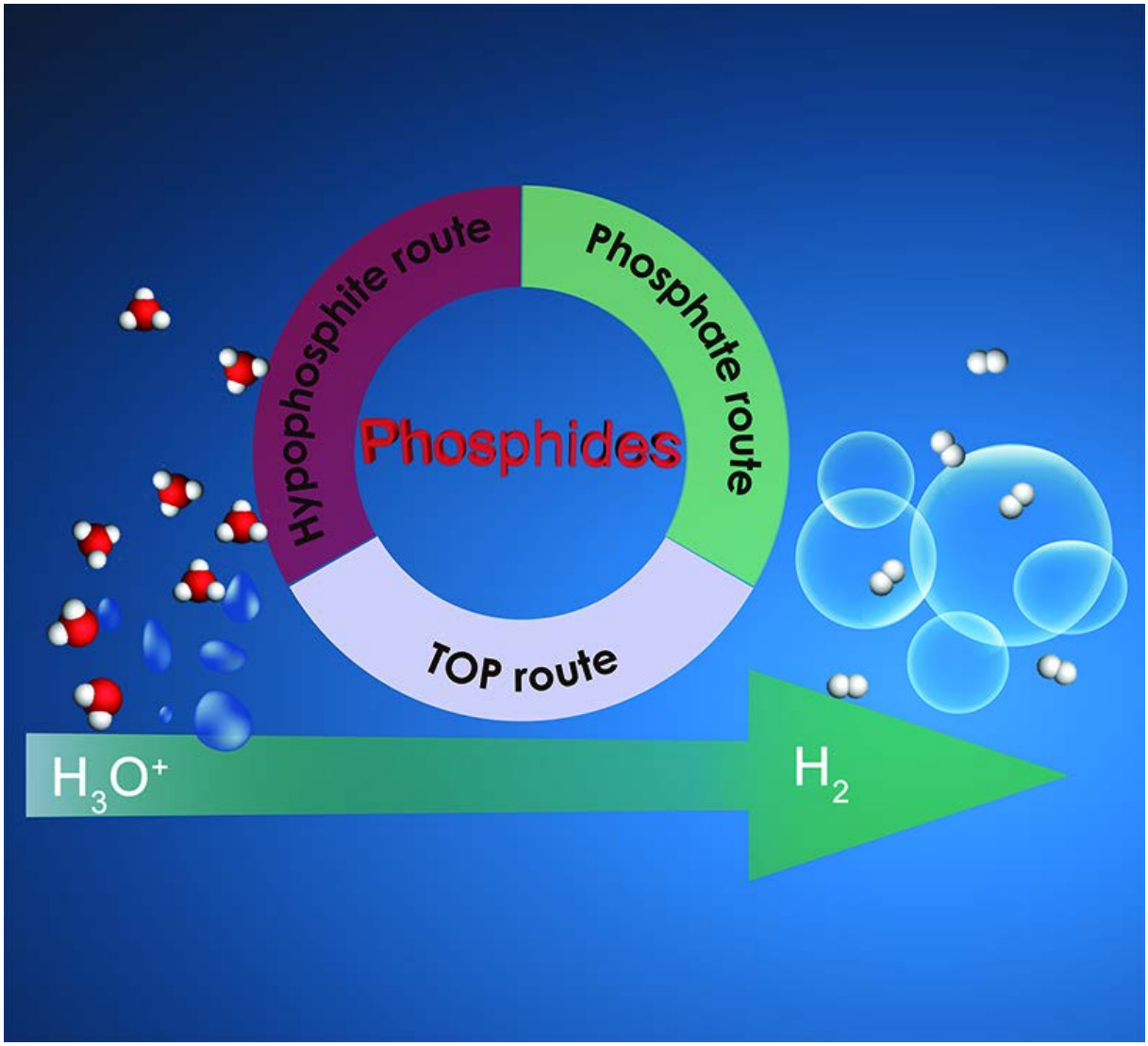
Hypophosphite route
Phosphate route
Phosphides
TOP route
H_3O^+
H_2

TOC Figure